Cross-linked Graphene Oxide Framework Membranes with Robust Nano-Channels for Enhanced Sieving Ability

Baoqiu Yuan[a], Mingxin Wang[a], Bo Wang[a], Fenglin Yang[a], Xie Quan[a], Chuyang Y. Tang[b]*, Yingchao Dong[a]*

[a] Key Laboratory of Industrial Ecology and Environmental Engineering (Ministry of Education, MOE), School of Environmental Science and Technology, Dalian University of Technology, Dalian 116024, China

[b] Department of Civil Engineering, The University of Hong Kong, Pokfulam, Hong Kong, China

***Corresponding author**:*

Prof. Chuyang Y. Tang
Department of Civil Engineering, The University of Hong Kong, Pokfulam, Hong Kong, China
Tel: +86-852-28591976 E-mail: tangc@hku.hk.

Prof. Yingchao Dong
Key Laboratory of Industrial Ecology and Environmental Engineering (Ministry of Education, MOE), School of Environmental Science and Technology, Dalian University of Technology, Dalian 116024, China
Tel: +86-411-84706328 E-mail: ycdong@dlut.edu.cn

Graphical Abstract

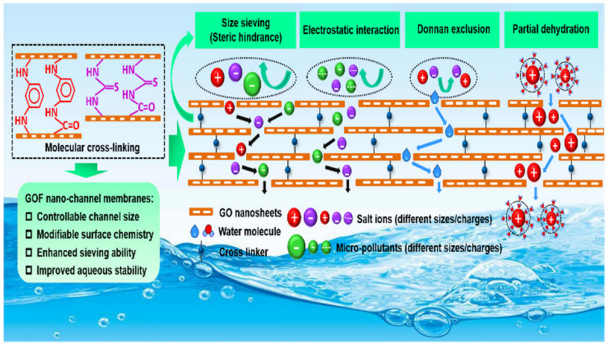

ABSTRACT

It remains challenging for graphene oxide (GO) membranes to achieve highly efficient performance and sufficient stability for aqueous molecule/ion precise separations. Herein, a molecular-level rational structure design protocol was proposed to develop ceramic-based graphene oxide framework (GOF) membranes with significantly enhanced sieving performance and stability for efficient removal of salts and micro-pollutants. Via a molecular cross-linking strategy, interlayered nano-channels between GO nanosheets can be rationally designed, featuring precisely tailorable channel size, promising surface chemistries and remarkably robust stability suitable for aqueous separation. Due to a significantly decreased nano-channel size, cross-linking of TU (thiourea) molecule significantly improved monovalent salt rejection (95.6% for NaCl), outperforming existing state-of-the-art GO-based, commercial organic nano-filtration and emerging two-dimensional MoS_2 membranes, while moderately decreasing water permeability. In comparison, the GOF membranes cross-linked with MPD (m-phenylenediamine) exhibited a simultaneous increase in permeability and rejection for both salts and micro-pollutants (21.0% and 53.3% enhancement for chloramphenicol (CAP) solution), breaking their conventional trade-off issue. Cross-linking mechanism indicates that more robust nano-channels were formed by stronger covalent bonds via dehydration condensation between amine (TU/MPD) and carboxyl groups (GO), and nucleophilic addition between amine (TU/MPD) and epoxy groups (GO). Molecule/ion separation mechanism involved size sieving (steric hindrance), electrostatic interaction, Donnan effect and partial

dehydration effect. This work provides a novel protocol for rationally designing size and surface chemistry of highly robust GO nano-channels at a sub-nanometer level to construct water-stable functional GOF membranes with enhanced sieving performance for water treatment applications.

INTRODUCTION

Severe water scarcity and pollution issues call for advanced purification technologies to produce potable clean water from unconventional sources such as wastewaters.[1] Considering their adverse health effect and ubiquitous presence in the environment,[2, 3] adequate removal of organic micro-pollutants such as antibiotics and endocrine disrupting compounds (EDCs), in addition to mineral salts, is essential for wastewater reclamation.[4, 5] Nanofiltration (NF) is considered to be a promising method for efficient removal of hazardous multi-valent salts and organic substances due to its unique advantages such as high separation efficiency, low energy consumption, small footprint, no phase change, environmental friendliness and continuous operational process.[6-9] In additional to a key challenging trade-off issue between permeability and selectivity, conventional nanofiltration membranes usually suffer from insufficient rejections especially for small-sized substances such as monovalent salts. More importantly, increasing selectivity is critically required for design of novel desalination membranes while there is limited impact of increased permeability on water purification efficiency.[10, 11] In spite of increasing applications in trace contaminant separation, traditional polymeric nanofiltration membranes still can

not perform well due to their insufficient stability and severe membrane fouling especially for more challenging applications such as treatment of pharmaceutical and aquaculture wastewaters with high-concentration pollutants/salts in harsh conditions (acidic, alkaline or organic-solvent). These limitations of existing nanofiltration membranes prompt us to rationally design and develop more robust membranes with enhanced separation performance.

In comparison, via environmentally sustainable organic-solvent-free synthesis routes,[12, 13] emerging two-dimensional (2D) graphene oxide (GO) nano-sheets can be feasibly assembled into GO framework (GOF) nano-filtration membranes since they are mechanically,[14] chemically and thermally robust,[15] and surface modifiable.[16-19] Generally, GOF membranes feature abundant separation-functional chemistry-size-designable 2D nano-channels which are periodically constructed by laminar GO nano-sheets via cross-linking or intercalating protocols, showing exceptional molecular or ion sieving ability for precise separations.[20] Ultra-fast water permeation inside nano-channels can be realized due to the preferential adsorption and rapid capillary diffusion of water molecules along GO nanosheet surface,[18, 20] enabling promising applications such as water/solvent separation,[21, 22] dye-wastewater purification,[23, 24] and seawater desalination.[25, 26] However, GOF membranes often suffer from their poor aqueous stability (i.e., severe swelling), insufficient selectivity or permeability especially for water treatment membrane systems under high pressure or long-term operation.[20, 27] Therefore, a key challenging issue is how to rationally structure-design GOF nano-filtration membranes finally exhibiting high selectivity

with acceptable permeability while enabling excellent long-term stability.[28-30]

Recently, via using novel cross-linkers with reactive groups, molecular cross-linking strategies have been used to precisely control the interlayer structure and separation performance (permeability and selectivity) of GO membranes, enabling various promising applications such as forward osmosis (FO), pressure retarded osmosis (PRO), pervaporation (PV) and NF.[20, 31-33] Different from state-of-the-art cross-linkers with other groups such as –COOH, -OH, -NCO and -CH_2Cl,[31, 34-36] cost-effective TU and MPD with active amine groups are expected to covalently cross-link terminal groups (such as carboxyl and epoxy) of GO nano-sheets to form more robust nano-channels. Moreover, their other inherent groups such as hydrophobic benzene rings would possibly endow a different nano-fluidic transport mechanism. Although their cross-linking could enhance PV and FO/PRO performance,[20, 31, 32] NF-based performance enhancement and space-confined transport mechanism have been not revealed in details for aqueous separation of high-concentration ions or pollutants in water via such a TU and MPD cross-linking strategy.

Herein we propose a molecular-level rational structure design protocol to develop ceramic-based GOF membranes with significantly enhanced sieving performance and stability for highly efficient removal of salt ions and emerging micro-pollutants. Via a molecular cross-linking strategy, interlayered nano-channels between GO nanosheets can be quantitatively designed, featuring precisely tunable channel size, promising surface chemistries and excellent long-term stability. In this work, thiourea (TU)

(76.12 Da) and m-phenylenediamine (MPD) (108.14 Da) molecules were used as covalent cross-linkers containing highly reactive binding sites to rationally construct highly robust GO nano-channels. In additional to remarkable long-term stability, the obtained GOF membranes exhibited enhanced removal performance for high-concentration salt ions and emerging micro-pollutants. The structural, physicochemical properties and separation performance (rejection and permeability) were characterized in details. Furthermore, cross-linking mechanism and separation models across functionalized GO nano-channels were proposed following detailed structural and performance characterizations. This work hopefully provides a novel protocol for rationally designing size and surface chemistry of robust GO nano-channels at a molecular level to construct stable functional GOF membranes with enhanced performance for water treatment applications.

MATERIALS AND METHODS

Fabrication and Modification of α-Al_2O_3 Substrates

Hollow fiber porous α-Al_2O_3 ceramic substrates were laboratory-prepared by a dry-wet spinning technique involving phase-inversion and sintering (Figures S1-S2 and Table S3). After optimizing preparation parameters such as spinning pressure and ethanol concentration (Figures S3-S4), the final α-Al_2O_3 substrates with excellent hydrophilicity (Figure S5) and mechanical properties (Figure S6) were used for the preparation of GO-based membranes (dimension: 1.8 mm outer diameter, 1.2 mm inner diameter, 60 mm length). The average pore size of α-Al_2O_3 ceramic substrate is 575±15 nm when sintered at 1550 ℃ (Figure S7). Then α-Al_2O_3 substrates were surface-modified with polydopamine (PDA) to improve the interfacial adhesion

between GO layer and the substrates according to the following procedures.[30] First, 80 mg dopamine hydrochloride was dissolved into 40 mL 10 mM Tris-HCl at pH 8.5 to prepare a solution (2 $mg \cdot mL^{-1}$) for subsequent impregnation. With both sides tightly sealed, the porous α-Al_2O_3 substrates were then immersed into the dopamine solution at 20 °C for 20 h and then dried at 60℃ for 24 h to allow a self-polymerization of dopamine, forming a PDA thin layer (~10 nm) on the surface of partially sintered alumina particles of the substrates. Finally, the modified substrates were rinsed using deionized (DI) water and fully dried at room temperature (25 °C) .[37-39] Compared with the untreated α-Al_2O_3 substrates, the PDA-modified substrates show slightly decreased water permeability (from 973.1 to 937.6 $Lm^{-2}h^{-1}bar^{-1}$ for Na_2SO_4 solution, from 924.5 to 903.2 $Lm^{-2}h^{-1}bar^{-1}$ for TC solution), and slightly increased rejection rate (from 0.02 to 0.03% for Na_2SO_4, from 0.03 to 0.04% for TC) (Figure S8). The key role of PDA layer was to only enhance the bonding force between substrate and GO while GO membranes actually played an role in ion/molecule separation, which was confirmed by significantly increased salt/pollutant rejection with much lowered permeability after coating GO layer (Figure S8).

Preparation of GO-based Membranes

GO, TU-GOF and MPD-GOF membranes were prepared on the PDA-modified α-Al_2O_3 substrates by simple vacuum filtration method using GO, TU-GO and MPD-GO suspensions (Figure 1 and Figures S9-S10). As shown in Figure S11, defect-free GOF membranes were prepared by vacuum filtration within only several minutes, the thickness of which could be controlled via changing filtration time (Figure S12). The resultant membranes were dried in an oven at 60 °C for 1 h.

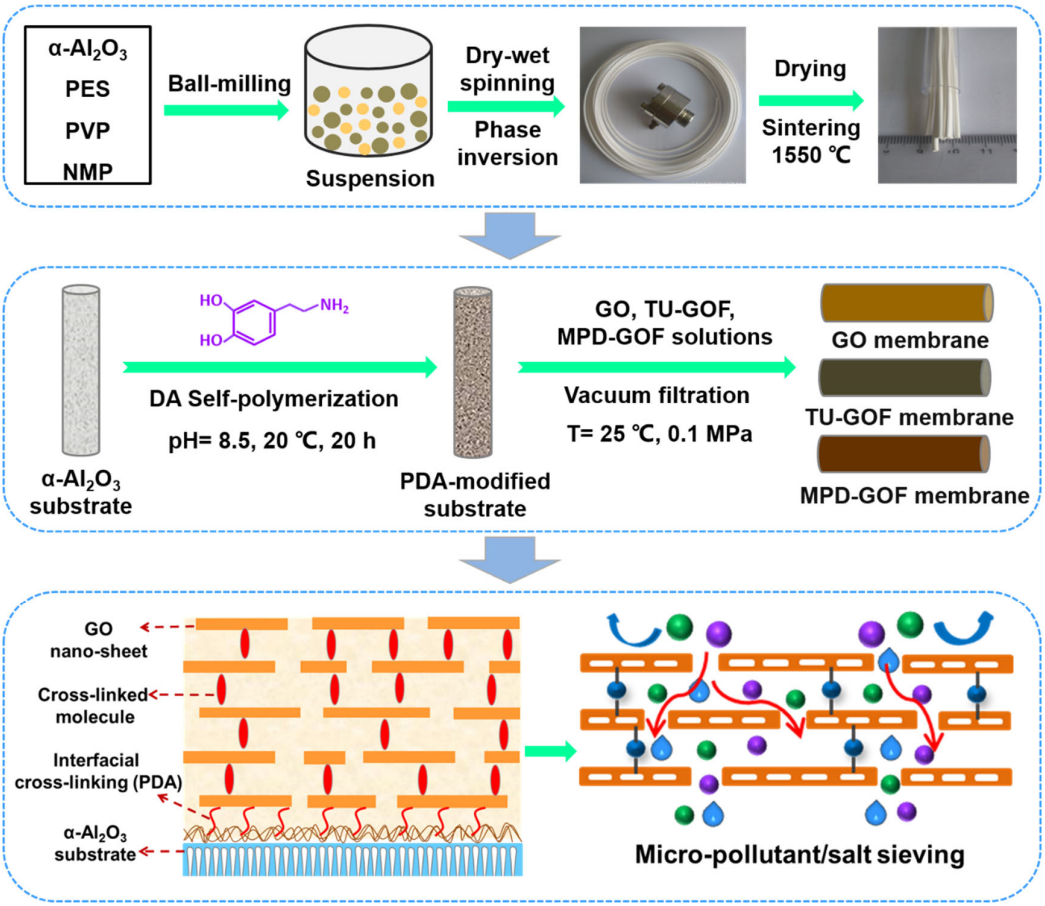

Figure 1. Schematic diagram of fabrication and separation application of TU- and MPD-functionalized GOF membranes on PDA-modified α-Al_2O_3 hollow fiber ceramic substrates.

Characterizations

The morphology and element composition of GO, TU-GOF and MPD-GOF membranes were characterized by field emission scanning electron microscope (FESEM, S-4800, Hitachi, Japan) equipped with energy dispersive spectrometer (EDS). Surface charge behaviors (zeta potential at different pH values) of GO-based suspensions were measured in a zeta-sizer instrument (ZS 90, Malvern Instruments Ltd., UK). The surface functional groups of GO, TU-GOF and MPD-GOF membranes were analyzed by Fourier transform infrared spectroscopy (FTIR, IS 50, Thermo

Nicolet, US) in the wavenumber range from 4000 to 800 cm^{-1} at room temperature (25 °C). X-ray photoelectron spectroscopy (XPS, Thermo Fisher, K-Alpha, US) was employed to characterize the surface compositions of the GO membranes, TU-GOF and MPD-GOF membranes at dry state. X-ray diffraction (XRD, D/Max 2400, Japanese Institute of Neo-Confucianism, Japan) was used to qualitatively identify crystalline phases, and quantitatively characterize the interlayer spacing of GO-based membranes with and without molecule-cross-linking. Interlayer spacing was calculated according to the Bragg equation (1):

$$2d \cdot sin\,\theta = n \cdot \lambda \quad (1)$$

where d (nm) is the interlayer spacing of GO nano-sheets in GO, TU-GOF and MPD-GOF membranes, θ is the diffraction angle, n is order of reflection (in general it is taken as 1), λ is the wavelength of X-ray (0.154056 nm).

Performance of GO-based Membranes

The separation performance of GO-based membranes (with the same membrane thickness) was tested in a homemade dead-end filtration device at room temperature (25 °C). All the membranes were first pre-run for 30 min before collecting permeates.[40] The transmembrane pressure applied during pre-run and permeation experiments was 0.5 MPa. The effective membrane area for separation was in the range of 1.9-2.3 cm^2. Water permeability J (L m^{-2} h^{-1} bar^{-1}) was calculated via the following equation (2):

$$J = \frac{V}{A \cdot \Delta t \cdot P} \quad (2)$$

where V is the permeate volume (L), A is the effective membrane area (m^2), Δt is collecting time interval (h), and P is the transmembrane pressure (bar).

To investigate separation performance, different micro-pollutants and salts were selected such as TC (Tetracycline, MW=444.43 Da), OTC (Oxytetracycline, MW=460.43 Da), CAP (Chloramphenicol, MW=323.14 Da), DS (Diclofenac sodium, MW=318.13 Da) (Tables S1-S2), Na_2SO_4, $MgSO_4$, $MgCl_2$ and NaCl for GO, TU-GOF and MPD-GOF membranes. The initial concentration of micro-pollutants was 50 $mg \cdot L^{-1}$ while that of salts was 100 $mg \cdot L^{-1}$. The pH of four salt solutions was 7.0 while those of four micro-pollutant solutions were 6.0, 8.0, 10.0 and 12.0 respectively. The duration of salt separation was 420 min while that of micro-pollutant separation was 240 min. Rejection was determined by the following equation (3):

$$R = \frac{C_f - C_p}{C_f} \times 100\% \quad (3)$$

where C_p ($mg \cdot L^{-1}$) and C_f ($mg \cdot L^{-1}$) are the permeate and feed concentrations of micro-pollutants or salt ions. The conductivities of the permeates and feeds were tested to determine salt concentration by a conductivity meter (DDSJ-308A, Shanghai REX Instrument Factory, China) (Figure S20). The concentrations of micro-pollutants were measured using a UV–visible spectrophotometer (Evolution 220, Thermo Fisher Scientific, US) at the wavelengths of 356, 353, 278 and 276 nm (Figure S21).

RESULTS AND DISCUSSION

Molecular Cross-linking of GO Nano-sheets

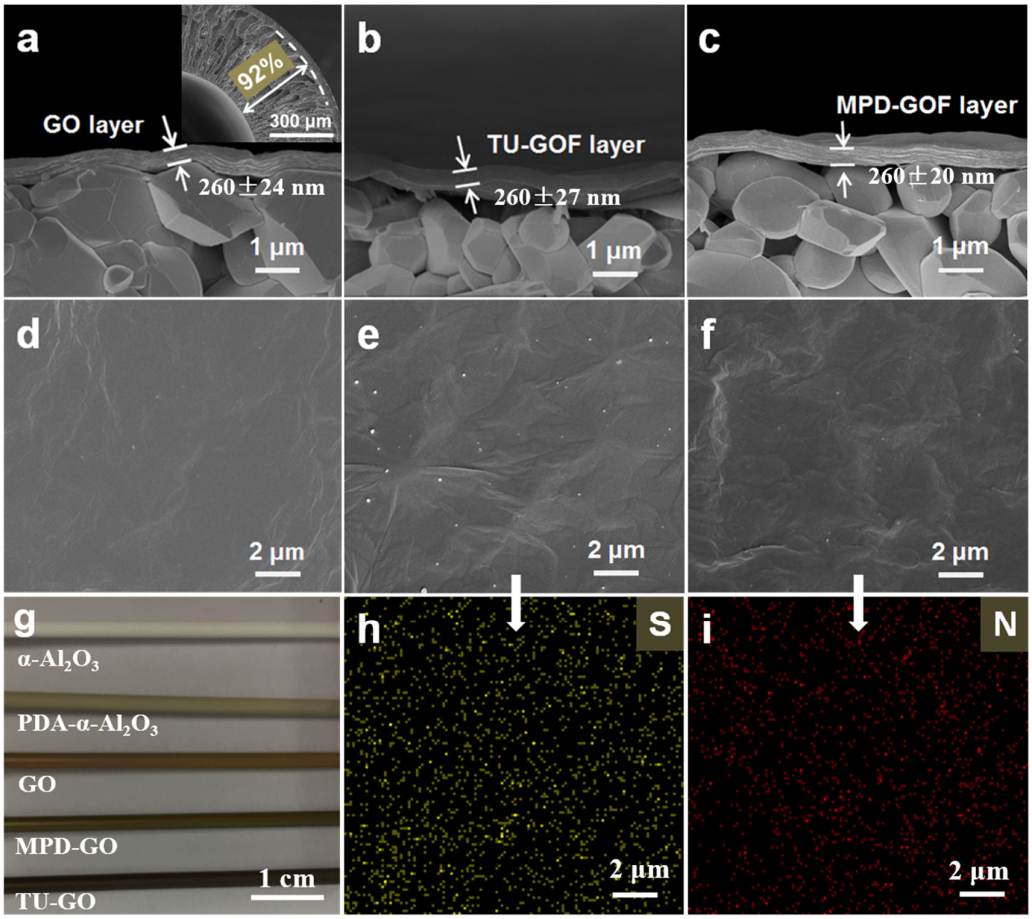

Figure 2. Cross-sectional (a, b, c) and top view surface (d, e, f) FESEM images of pristine GO membrane (a, d), TU-GOF (b, e) and MPD-GOF (c, f) membranes. The inset in Fig. 2a shows the cross-sectional SEM image of α-Al_2O_3 substrate. (g) Optical image of α-Al_2O_3 substrate, PDA-modified α-Al_2O_3 substrate, pristine GO membrane, MPD-GOF membrane, and TU-GOF membrane. (h) S-element (yellow signal) EDS mapping image of TU-GOF membrane surface. (i) N-element (red signal) EDS mapping image of MPD-GOF membrane surface.

The final α-Al_2O_3 substrates exhibited a typical asymmetric structure consisting of ultra-long finger-like macrovoids (~92%) and a thin sponge-like layer (~8%) (inset in

257 Figure 2a). Such an ultra-long finger-like macrovoid structure, combined with
258 excellent hydrophilicity (water contact angle ~20°, Figure S5), was beneficial to
259 improve water permeability of the substrates due to significantly reduced mass
260 transport resistance.[41] Membrane thickness and water permeability could be regulated
261 by controlling filtration time (Figure S12). After vacuum filtration, pristine GO,
262 TU-GOF and MPD-GOF membranes all have a well-stacked two-dimensional
263 laminar structure with the same thickness (GO ~260±24 nm; TU-GOF ~260±27 nm;
264 MPD-GOF ~260±20 nm), which were tightly coated on the ceramic substrate
265 surfaces with enhanced interfacial bonding via a self-polymerization of dopamine
266 (Figures 2a-2c). They also show an integrate membrane surface morphology featuring
267 continuous coverage, no visible defects and pinholes (Figures 2d-2f). Compared to
268 brown-colored pristine GO membrane (Figure 2g), the surfaces of black TU-GOF and
269 darker brown MPD-GOF membranes look rougher with typical wavy-wrinkles and
270 homogeneous molecular incorporation (Figures 2h-2i). Such a color change based on
271 the same thickness preliminarily indicates that MPD and TU reacted with oxygenated
272 groups of GO nano-sheets via molecular cross-linking, resulting in a decrease in
273 oxygen content (will discuss in the following section).

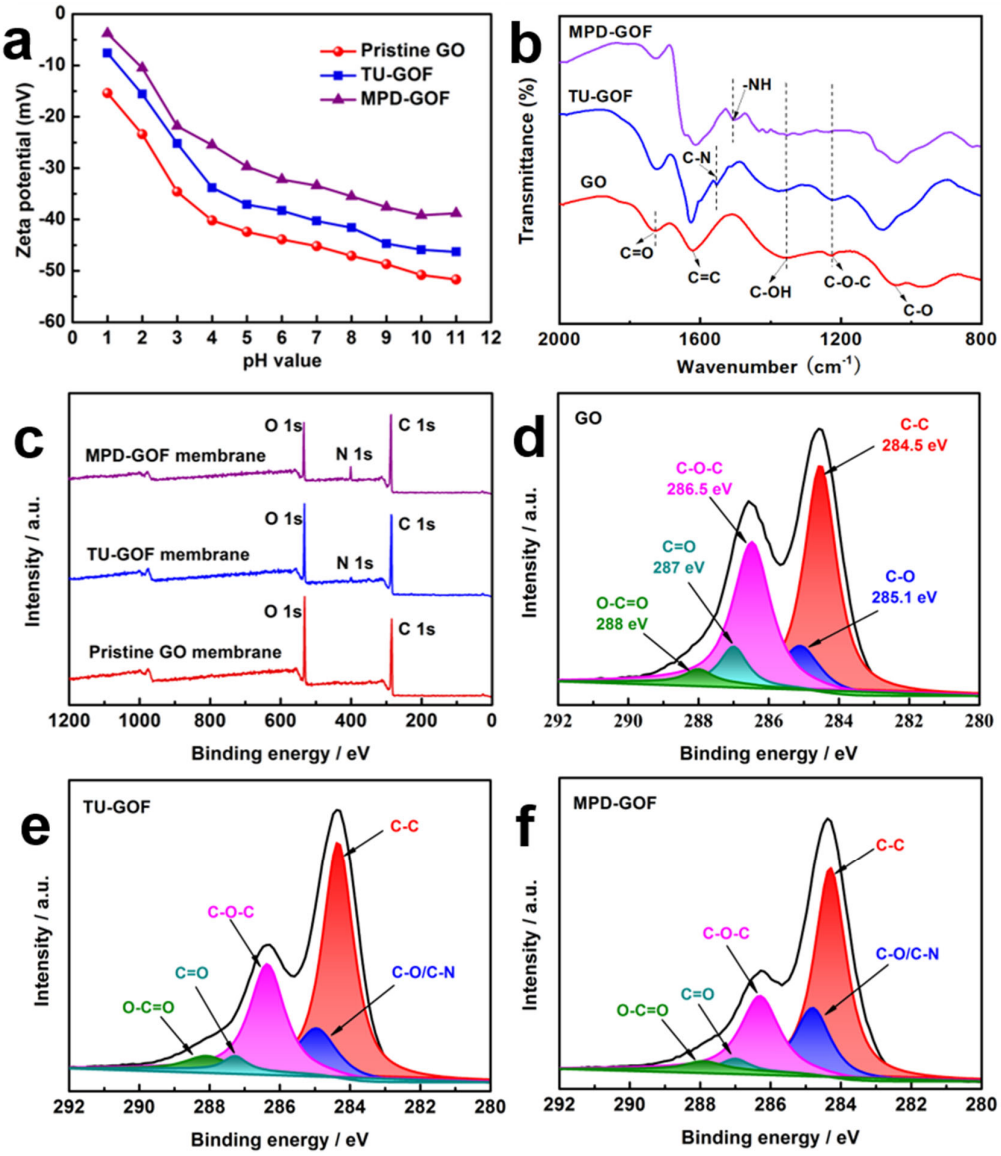

Figure 3. Chemical properties of pristine GO, TU-GOF and MPD-GOF membranes. (a) Zeta potential under different pH values and (b) FTIR spectra in the wavenumber range of 2000-800 cm^{-1}; (c) XPS wide scan, and XPS narrow scans for C1s peaks for GO (d), TU-GOF (e) and MPD-GOF (f) membranes.

In a wide pH range from 1 to 11, pristine GO, TU-GOF and MPD-GOF nano-sheets are all negatively charged (Figure 3a) due to the deprotonation reaction of inherent carboxyl groups on GO surface.[42, 43] Compared to pristine GO, the negative charges of TU-GOF and MPD-GOF are slightly suppressed because cross-linking reactions of

TU and MPD with GO nano-sheets consumed their partial carboxyl groups with additional amine groups.[20, 30] For pristine GO membranes, the adsorption bands of C=O stretching (1727 cm^{-1}), sp^2–hybridized C=C (1621 cm^{-1}), C-OH stretching (1354 cm^{-1}), C-O-C stretching (1225 cm^{-1}) and C-O stretching (1045 cm^{-1}) are clearly identified respectively (Figures 3b, S13 and Table S4), which can be ascribed to carbonyl/carboxyl, aromatic, carboxyl, epoxy and alkoxy groups on GO nano-sheets.[44-46] In comparison, for TU-GOF membrane, in spite of constant peak intensity of C-OH stretching (1354 cm^{-1}), the absorption peak intensities of C=O stretching (1729 cm^{-1}) and C-O-C stretching (1225 cm^{-1}) are decreased, indicating again a partial consumption of their corresponding oxygenated groups via cross-linking reaction between TU and GO. After cross-linking with TU, the adsorption band of C=O stretching vibration slightly blue-shifted from 1727 to 1729 cm^{-1}, which has been well confirmed in other reports.[35, 47, 48] In addition, the formation of a new band at 1553 cm^{-1} can be ascribed to the antisymmetric C–N stretching coupled with out-of-plane NH_2 and NH modes.[49] This indicates again that TU was covalently crosslinked onto GO nano-sheets. Similarly, for MPD-GOF membrane, the peak intensities of carboxyl (C=O stretching at 1727 cm^{-1} and C-OH stretching at 1354 cm^{-1}), and epoxy (C-O-C stretching at 1225 cm^{-1}) groups are greatly suppressed. Furthermore, a new peak arises at 1507 cm^{-1}, which can be assigned to the C-N stretching and C-NH deformation vibrations.[46] This demonstrates that amine groups in TU/MPD reacted with GO carboxyl groups via dehydration condensation and GO epoxy groups via nucleophilic addition reaction, consequently consuming oxygenated

functional groups on GO nanosheets.[44, 50]

XPS analysis was used to further confirm the cross-linking reaction between TU or MPD and GO nano-sheets for dry-state GO, TU-GOF and MPD-TOF membranes.[20, 44] C1s and O1s peaks are observed in all three membranes, while N1s peak is identified for both TU-GOF and MPD-GOF membranes because of the formation of amide (-CO-NH-) groups (Figure 3c). Moreover, compared to pristine GO membrane (O/C ratio ~0.38), the O/C ratios in TU-GOF and MPD-GOF membranes are decreased to 0.32 and 0.26, respectively (Table S5). Such a decrease in O/C ratio resulted from the consumption of oxygenated groups (carboxyl and epoxy groups) of GO by their reactions with TU and MPD molecules, which is consistent with the FTIR results (Figure 3b and Figure S13). As shown in Figure 3d, the C1s spectra of pristine GO membrane can be deconvoluted into five characteristic peaks at binding energies of 284.5, 285.1, 286.5, 287 and 288.1eV, which correspond to C-C/C=C, C-O/C-N, C-O-C, C=O and O-C=O, respectively. However, compared to pristine GO membrane, the peak intensity of C-O-C and O-C=O bands exhibites a significant decline for TU-GOF membrane (Figure 3e, Figure S14 and Table S6), which once again indicates a partial consumption of epoxy and carboxyl groups. Futhermore, the intensity of C-O/C-N peak is increased significantly owing to the formation of a new C-N covalent bond (Figure 3f, Figure S14 and Table S6), which once more confirms that the amine groups in MPD reacted with carboxyl and epoxy groups on GO to form covalent bonds via dehydration condensation and nucleophilic addition reaction respectively. Cross-linking mechanism of GOF-based membranes was further

confirmed by their S2p and N1s narrow scan spectra (Figure S15), clearly indicating the formation of new amide group (C-NH bonding at 400.2 eV) in both TU-GOF and MPD-GOF membranes via covalent cross-linking reactions.

Regulatable Nano-channel Size and Enhanced Stability

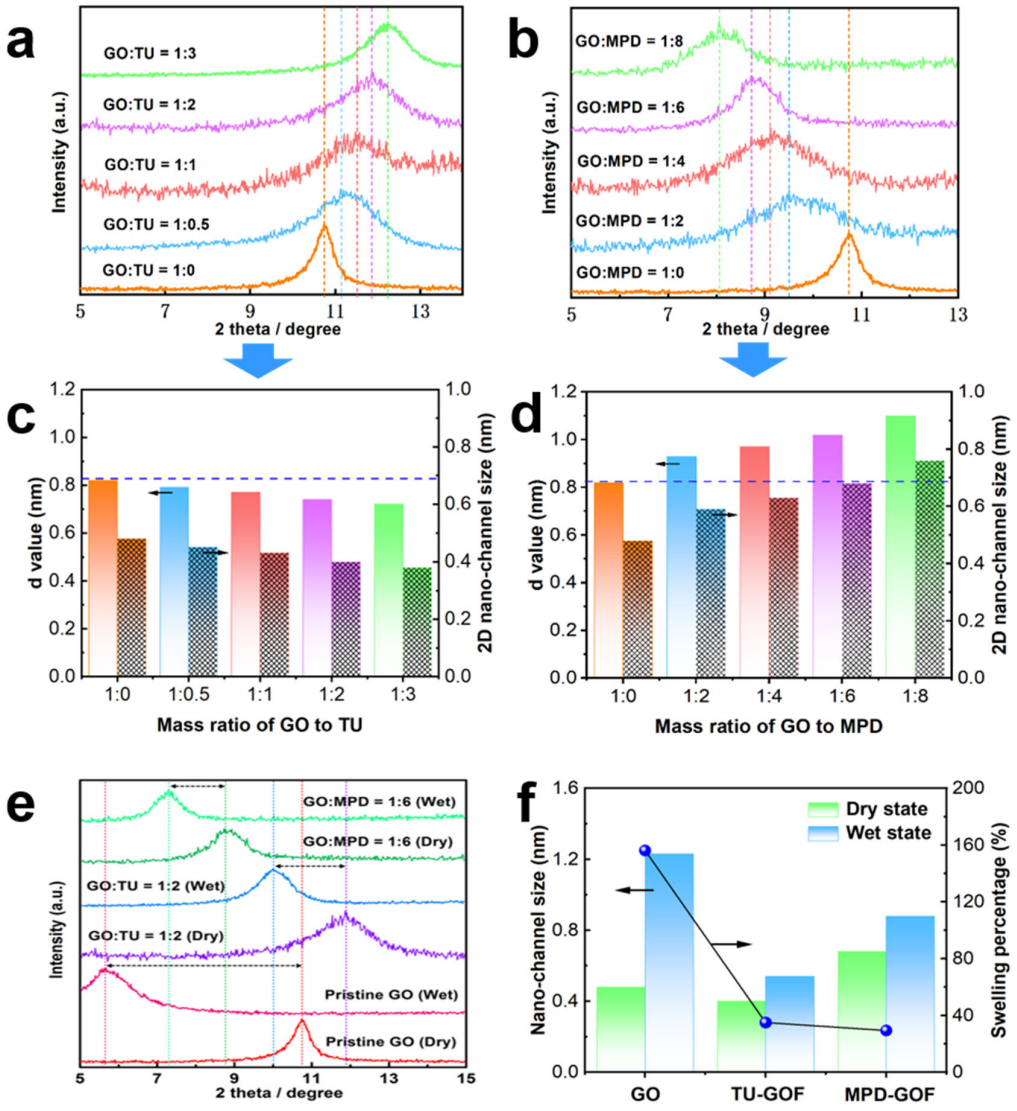

Figure 4. Phase structure, interlayer spacing and nano-channel size of the GOF membranes covalently cross-linked with TU and MPD molecules at dry and wet states. (a) XRD patterns, and (c) interlayer spacing (d-spacing) value and 2D nano-channel size of pristine GO membrane (GO:TU=1:0) and TU-GOF membranes with different GO/TU mass ratios at dry state; (b) XRD patterns and (d) interlayer spacing (d-spacing) value and 2D nano-channel size

337 of pristine GO membrane (GO:MPD=1:0) and MPD-GOF membranes with different
338 GO/MPD mass ratios at dry state; (e) XRD patterns and (f) 2D nano-channel size and its
339 swelling percentage of pristine GO, TU-GOF (GO:TU=1:2) and MPD-GOF (GO:MPD=1:6)
340 membranes which were altered from dry to wet state.

341 Both interlayer spacing and nano-channel size of GOF-based membranes can be
342 precisely regulated at a sub-nanometer level via such a covalent cross-linking strategy
343 (Figure 4). Cross-linking of adjacent GO nano-sheets via TU molecule resulted in a
344 gradual decrease in the size of both interlayer spacing and GO nano-channels at dry
345 state (Figures 4a and 4c), where GO single layer size (~0.34 nm) was deducted for the
346 latter.[18] Via dehydration condensation between -NH_2 (TU) and -COOH (GO) as well
347 as nucleophilic addition between -NH_2 (TU) and C-O-C (GO), TU cross-linking
348 between adjacent GO nano-sheets periodically resulted in structurally narrowed
349 well-defined 2D nano-channels (interlayer spacing as well) due to the small
350 dimension of covalent TU-link and the deoxygenation of –COOH group.[20] A
351 nano-channel size of 0.48 nm was determined for pristine GO membrane, while that
352 of TU-GOF (1:0.5) membrane is slightly decreased to ~0.45 nm (Figure 4c). Such a
353 gradual decrease in nano-channel size ranging from ~0.48 nm (GO:TU=1:0) to ~0.38
354 nm (GO:TU=1:3) was beneficial to improve membrane selectivity. In comparison, for
355 MPD-GOF membranes at dry state, 2D nano-channel size increased gradually in the
356 range of 0.48-0.76 nm with decreasing GO:MPD ratio from 1:0 to 1:8 after
357 cross-linking (Figures 4b and 4d). Such a gradually enlarged nano-channel size is
358 expected to facilitate membrane permeability. Compared with small-sized TU
359 molecule (76.12 Da), cross-linking via larger-sized MPD (108.14 Da) resulted in a

larger interlayer spacing (0.74 nm vs. 0.93 nm) for GOF membranes with the same loading (GO:TU= 1:2 vs. GO:MPD= 1:2) at dry state. After robust covalent cross-linking, the WCA of both TU-GOF and MPD-GOF membranes increased (~72°-82° vs. ~56° and ~75°-85° vs. ~56°), indicating reduced hydrophilicity (Figure S16).

Aqueous stability is a key challenging issue for practical water treatment applications of GO-based membranes. However, when pristine GO membranes were immersed into water, their nano-channel size significantly increased from 0.48 nm to 1.23 nm, indicating a severe swelling phenomenon (with a swelling ratio as high as ~156%) (Figures 4e-4f and Table S7). This unfavorable swelling can be ascribed to the weak interaction (i.e., electrostatic repulsion mechanism) between adjacent GO nanosheets when excessive water molecules were easily captured inside GO nano-channels by the strong hydration enabled by plentiful oxygenated functional groups on pristine GO nanosheets. In our work, although PDA modification enhanced interfacial bonding between ceramic substrate and GO layer,[23, 30] an undesirable disruption of membrane structure was visibly observed after static soaking in acidic or alkaline solutions for only 7 days due to its severe swelling with excessive nano-channel/interlayer-spacing enlarging (Figure S17), definitely significantly degrading performance such as selectivity and long-term stability (Figure S18).

By comparison, interestingly, molecular covalent cross-linking via TU and MPD could tightly interlock GO nano-sheets against this swelling tendency (Figures 4e-4f and Figures S17-19). Their nano-channel size more slightly increased only from 0.40

382 to 0.54 nm (TU-GOF membrane), from 0.68 to 0.88 nm (MPD-GOF membrane) with
383 significantly suppressed swelling ratios of only ~35% and ~29% from dry to wet state
384 (Figures 4e-4f and Table S7), fully demonstrating their excellent anti-swelling ability
385 in aqueous solutions via the formation of highly robust confined nano-channels.
386 Cross-linking using TU and MPD consumed the oxygenated groups on GO
387 nano-sheets (Figures 3b-3c), resulting in not only a reduction in electrostatic repulsion
388 but the formation of stronger covalent bonds between adjacent GO nano-sheets,
389 consequently prohibiting membrane swelling with suppressed nano-channel
390 dimension. Both TU-GOF and MPD-GOF membranes exhibited extraordinary
391 aqueous stability and robustness with much better structural integrity not only in
392 water, but also in strong acidic (HCl, pH = 1) and basic (NaOH, pH = 11) solutions,
393 even after more than three months (Figure S17). In addition, during long-term
394 operation, TU-GOF, MPD-GOF membranes exhibited time-dependent slight decrease
395 (but acceptable stability) in permeability and salt rejection (Figure S18d).
396 Nevertheless, compared with GO, the prepared GOF membranes (TU-GO and
397 MPD-GO) had better long-term stability in Na_2SO_4 rejection due to their more robust
398 nano-channels after TU or MPD cross-linking (Figure S18d). The key concerns of our
399 current work focus on performance (permeability and selectivity) enhancements,
400 cross-linking and separation mechanisms at lab scale. Following this work, more
401 future efforts should be systematically performed to further improve its longer-term
402 performance and stability for both salts and pollutants.

403 **Enhanced Salt and Pollutant Sieving Performance**

404 Salt ion sieving ability is an essential indicator for evaluating nanofiltration
405 membranes.[51] Pristine GO membranes exhibited moderate rejections for Na_2SO_4 (72.6

406 ± 1.1%), $MgSO_4$ (58.4 ± 1.8%), NaCl (45.8 ± 1.3%), and $MgCl_2$ (23.7 ± 2.5%)
407 following an order of R (Na_2SO_4) > R ($MgSO_4$) > R (NaCl) > R ($MgCl_2$) (Figure 5a),
408 which are at similar levels with previous reports.[30, 52] This phenomenon can be
409 explained via size sieving and Donnan exclusion effects. The negatively charged
410 GO-based membrane tended to repel salt ions such as SO_4^{2-} and Cl^- from membrane
411 surface. However, in order to maintain the electro-neutrality for both feed and
412 permeate solutions, the counter ions such as Mg^{2+} and Na^+ were rejected. According
413 to the Donnan exclusion theory (Eq. 4),[9, 29] rejection is related to ionic valence,
414 following the order of the ratio of $Z^{\text{co-ions}}$ to $Z^{\text{counter ions}}$, where Z is the ionic valence.

415 $$R = 1 - \frac{C_B^m}{C_B} = 1 - \left(\frac{|Z_B| C_B}{|Z_B| C_B^m + C_X^m} \right)^{|Z_B|/|Z_A|}$$

416 (4)

417 Where Z_A and Z_B are the valences of counter ions (positively charged ions) and
418 co-ions (negatively charged ions), respectively, C_B (mol·L^{-1}) and C_B^m (mol·L^{-1})
419 are the concentrations of co-ions in solution and membrane phase, respectively, and
420 C_X^m is the membrane charge concentration. Theoretically, salt rejection should follow
421 this order R (Na_2SO_4) > R ($MgSO_4$) ≈ R (NaCl) > R ($MgCl_2$). However, despite
422 having the same valence ratio of anion to cation, a higher rejection was detected for
423 $MgSO_4$ (58.4 ± 1.8%) than NaCl (45.8 ± 1.3%) in the experiment, which was
424 attributed to a more dominant role of size sieving effect. Compared with Na^+ ($R_{hydrated}$
425 0.36 nm) and Cl^- ($R_{hydrated}$ 0.33 nm), large-sized hydrated Mg^{2+} ($R_{hydrated}$ 0.43 nm) and
426 SO_4^{2-} ($R_{hydrated}$ 0.38 nm) were more easily blocked by GO nano-channels.[53, 54]

427 After TU cross-linking, due to a remarkable suppressing in nano-channel size (from

1.23 to 0.54 nm, Figure 4f and Table S7), a significant enhancement in salt rejection was achieved for TU-GOF membrane (GO:TU=1:2), showing an almost complete rejection for Na_2SO_4 and $MgSO_4$ while very high rejection for NaCl (95.6 ± 1.14%) and $MgCl_2$ (90.2 ± 0.95%) (Figure 5b). Despite lowering water permeability, increasing selectivity is more highly required for design of high-performance desalination membranes since there is limited impact of increased permeability on water purification efficiency.[10, 11] Such high rejections of NaCl not only far exceeded those of pristine GO membranes, but other reported state-of-the-art GO-based, commercial organic nano-filtration and emerging two-dimensional MoS_2 membranes which all operated under the same NF mode (Figure 5e and Table S8). Generally, only reverse osmosis (RO) or FO membranes can fully reject NaCl while most NF membrane can not perform well.[19, 55, 56] In spite of significantly enhanced ion rejection, minor Na^+ (4.4 ± 1.1%, NaCl) and Mg^{2+} (9.8 ± 0.9%, $MgCl_2$) ions with larger size still passed across smaller TU-GOF membrane nano-channels. Both hydrated Na^+ ($D_{hydrated}$ 0.72 nm) and Mg^{2+} ($D_{hydrated}$ 0.86 nm) ions have larger size than the nano-channels (~0.54 nm) of TU-GOF membrane at wet state while dehydrated Na^+ ($D_{dehydrated}$ 0.19 nm) and Mg^{2+} ($D_{dehydrated}$ 0.53 nm) ions have smaller size.[57, 58] That is so say, the pore diameter of TU-GOF nano-channels was smaller than hydrated ionic diameter but larger than dehydrated ionic diameter. We can thus speculate that its ion separation performance should be dominated by a combined mechanism of size sieving associated with partial dehydration effect,[57, 59] where large-sized hydrated ions should undergo a dehydration mechanistic process to enter the nano-channels, which

has been widely confirmed in the ion channels of GO, biological or metal-organic frameworks membranes.[58] When dehydrated ions exited the nano-channels and entered an aqueous solution, they were rehydrated by water molecules. Nevertheless, such a significant rejection enhancement was at the cost of moderate permeability decrease (Figure 5b). Interestingly, after cross-linking with MPD molecules, MPD-GOF membranes (GO:MPD=1:4) exhibited a simultaneous enhancement in rejection and permeability for four salts (Figures 5c-5d). Cross-linking with MPD indeed enlarged nano-channel size at dry state, but significantly suppressed it at wet state in the actual NF process (Figure 4). Covalent cross-linking of adjacent GO nano-sheets enhanced not only the aqueous robustness of nano-channels with longer-term stability for more than three months (Figure S17), but their salt sieving ability in both rejection and permeability (Figure S18). Enhanced rejection (for instance, from 45.8% to 75.2% for NaCl, from 72.6 to 93.5% for Na_2SO_4) can be ascribed to reduced aqueous nano-channel dimension as well as an additional steric hindrance mechanism of decorated larger-sized MPD molecules with benzene rings, thus effectively blocking (i.e. rejecting) small-sized salt ions. In spite of suppressing wet-state nano-channel dimension after MPD cross-linking (Figure 4f), an extraordinary enhancement in water permeability was observed (Figure 5d) (will discuss in the following section).

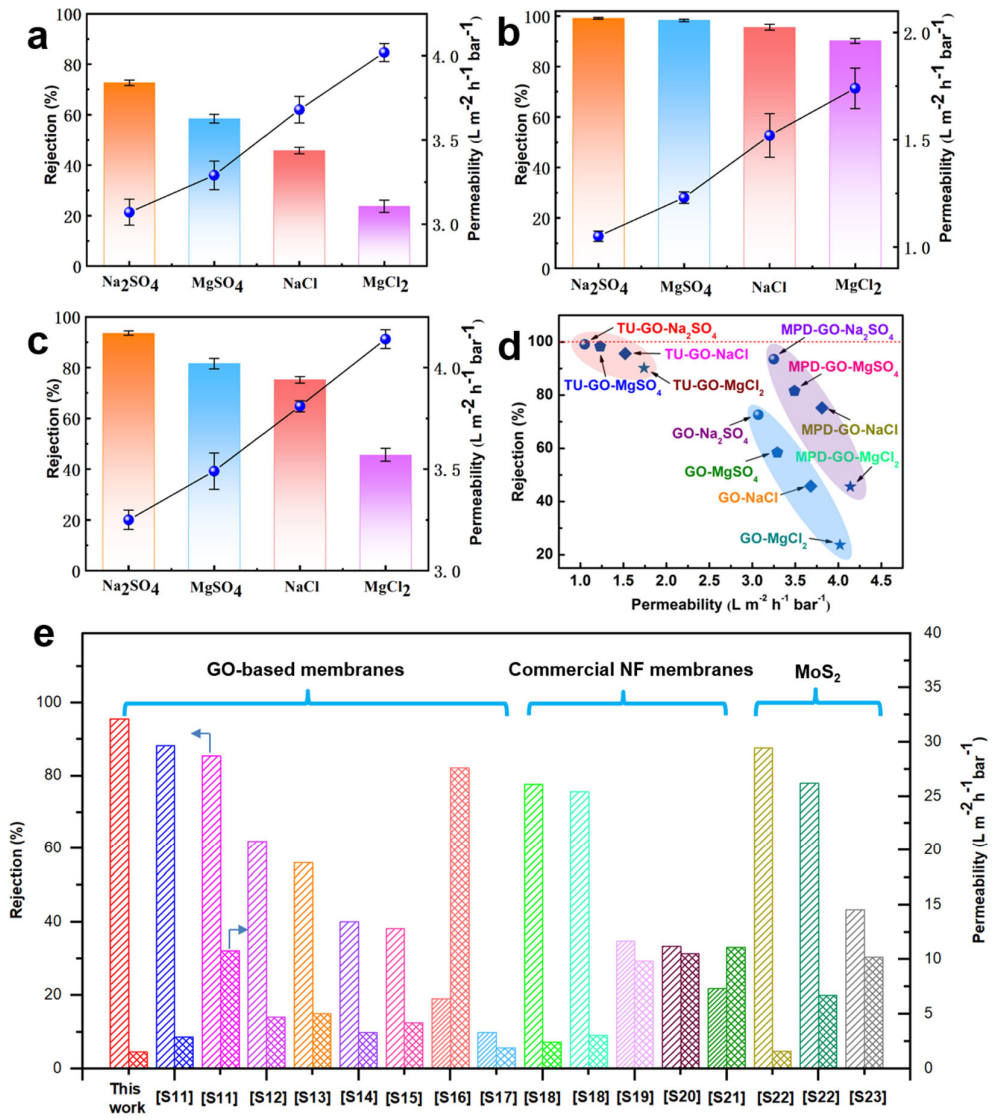

Figure 5. Rejection and permeability of pristine GO membranes (a), TU-GOF (b), and MPD-GOF (c) membranes with the same thickness for separation of four different salt solutions with a constant concentration of 100 mg·L^{-1}; (d) Comparison of salt sieving performance (rejection and permeability) of GO, TU-GOF and MPD-GOF membranes; (e) Comparison of NaCl rejection and water permeability between TU-GOF membrane in this work, and other state-of-the-art GO-based membranes, commercial NF membranes and two-dimensional MoS_2 membranes which operated in NF mode. (See more reference in Table S8, Supporting information)

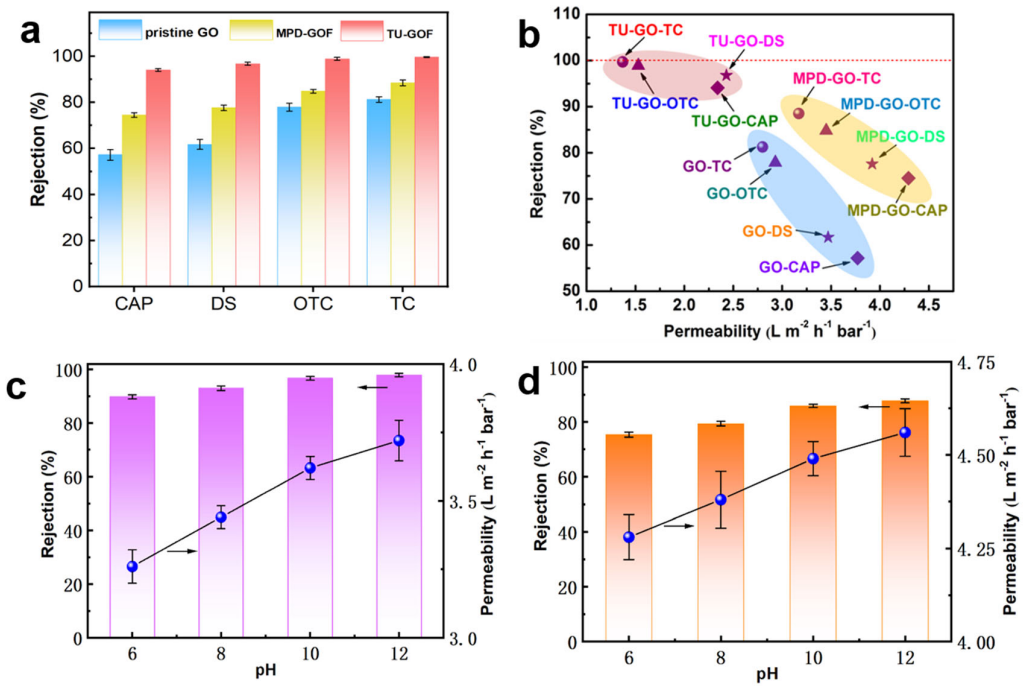

Figure 6. (a) Pollutant rejection of pristine GO membranes, TU-GOF membranes with a GO/TU mass ratio of 1:1 and MPD-GOF membranes with a GO/MPD mass ratio of 1:6; (b) Performance comparison in permeability and rejection of three types of GO-based membranes for removal of four micro-pollutants. The applied trans-membrane pressure was 5 bar and the feed concentration was 50 mg·L^{-1} for four micro-pollutants; (c) Permeability and rejection of MPD-GOF membranes with a GO/MPD mass ratio of 1:6 for removal of TC at different pH values; (d) Permeability and rejection of MPD-GOF membranes with a GO/MPD mass ratio of 1:6 for removal of CAP at different pH values.

In addition to salt sieving, we also further evaluated the micro-pollutant separation performance for GO, TU-GOF and MPD-GOF membranes. For four selected typical micro-pollutants, the size shows an order DS < CAP < TC < OTC in MW (Table S2). Pristine GO membranes exhibit low rejections (57.2 ± 2.3% for CAP, 61.7 ± 2.1% for DS) for smaller-sized CAP and DS but higher rejections (77.9 ± 1.7% for OTC, 81.3 ± 1.2% for TC) for larger-sized OTC and TC (Figure 6a). Compared to rejection, an opposite trend is observed for water permeability (Figure 6b). After cross-linking with

494 TU (CH_4N_2S, 76.12 Da) (Figures 6a and S22a), like salt rejection (Figure 5), the
495 TU-GOF membranes show a significant increase in CAP rejection due to the
496 enhanced steric hindrance effect via reducing nano-channel size (Figures 4a and 4c).
497 A complete CAP rejection (99.9 ± 0.1%) was achieved at GO/TU 1:3, much higher
498 than 57.2 ± 2.3% at GO/TU 1:0 (pristine GO membrane) (Figure S22a). Similarly,
499 rejections were also significantly improved for DS (96.8 ± 0.7%), OTC (98.9 ± 0.6%)
500 and TC (99.7 ± 0.2%) (Figure 6a). In spite of significantly enhanced rejection,
501 however, the water permeability is sacrificed for TU-GOF membranes (like salt
502 sieving in Figure 5).

503 In order to address this issue, larger size MPD ($C_6H_8N_2$, 108.14 Da) with active
504 functional groups ($-NH_2$) and benzene rings was then introduced as a cross-linker into
505 GO membrane (Table S2). Interestingly, compared with pristine GO membranes, like
506 salt separation (Figure 5), the MPD-GOF membranes with a GO/MPD mass ratio of
507 1:6 show simultaneous increases in rejection and water permeability for CAP, DS,
508 OTC and TC solutions, breaking their conventional trade-off issue (Figures 6 and
509 S22b). Unlike that cross-linking with TU only significantly enhanced rejection with a
510 moderate sacrifice of water permeability (Figure 6b), cross-linking with MPD resulted
511 in simultaneously enhanced rejection and water permeability via reducing GO
512 nano-channel size inside the wet membranes. The water permeability increases with
513 MPD content especially at GO:MPD ratios < 1:4 while maintaining high CAP
514 rejection. At GO:MPD = 1:8, MPD-GOF membrane exhibits an enhanced water
515 permeability of 5.38 ± 0.07 L m^{-2} h^{-1} bar^{-1} (1.43 times higher than pristine GO

membrane) and CAP rejection of 70.8 ± 1.3% (Figure S22b). Like salts, such a moderate decrease in nano-channel size (from 1.23 to 0.88 nm) led to moderately improved rejection for micro-pollutants. However, this decrease in nano-channel size additionally improved, not lowered water permeability, which is different from a generally acceptable viewpoint that a decrease in pore size inevitably causes a permeability loss. In addition, for MPD-GOF membranes, a gradual enhancement is observed in both rejection and water permeability with increasing pH value (TC in Figure 6c, CAP in Figure 6d). This simultaneous improvement can be attributed to an enhanced electrostatic repulsion interaction between MPD-GO membrane and TC/CAP molecules, i.e., more negatively charged (Figure 3a).[5] Ionization state of antibiotics in water is usually affected by pH value, which is reflected by a property indicator named as dissociation constant pKa. As an amphoteric compound, TC is positively charged below pH 3.32 but negatively charged above pH 7.78, and consequently neutrally charged within a pH range of 3.32–7.78.[60] At pH=6, a relatively low rejection rate (89.7%) of neutrally charged TC is observed, which was dominated by a size sieving mechanism. With pH value increased from 6 to 12, a gradual rejection enhancement is observed due to an enhanced electrostatic repulsion mechanism associated with size sieving. A similar trend can also be observed in CAP rejection (Figure 6d), where CAP is positively charged below pH=2 but negatively charged above pH=9, and consequently neutrally charged within a pH range of 2–9. At high pH condition, electrostatic repulsion was enhanced between adjacent GO nano-sheets, therefore expanding nano-channels to increase water permeability.[61]

Mechanistic Insight for Robust Cross-linking and Enhanced Sieving

A mechanistic insight is proposed here to understand molecular cross-linking and salt/molecule sieving for robust space-confined nano-channels in GOF membranes (Figure 7). Molecular covalent cross-linking between TU or MPD and GO nano-sheets mainly involved carboxyl and epoxy groups via dehydration condensation and nucleophilic addition reaction, respectively. Based on XPS C1s peak (Figures 3d-3f), more epoxy groups (~34%) were dominantly detected on GO nano-sheets than carboxyl (~2%) (Table S6). Since hydroxyl and carboxyl groups are located around the edges of GO nano-sheets while carbonyl and epoxy groups are concentrated at their interior planes,[62, 63] we can speculate that after cross-linking reactions TU and MPD molecules more dominantly exist on the interior planes than the edges (Figure 7b). Via a covalent cross-linking strategy, amine groups ($-NH_2$) in TU and MPD molecules provided highly active binding sites to react with GO carboxyl groups through dehydration condensation reaction, and GO epoxy groups through nucleophilic addition reaction (Figures 7a-7b). Such a covalent cross-linking was beneficial to not only regulate the size of GO nano-channels more stably formed between adjacent GO nano-sheets, but tailoring their surface chemistries (such as surface terminal groups, hydrophilicity/hydrophobicity and surface charges). Moreover, due to its much higher bond energy, this chemically covalent cross-linking was much stronger than hydrogen bond or van der Waals force, significantly suppressing electrostatic repulsion between adjacent GO nano-sheets, which was a key action force responsible for severe swelling of pristine GO membranes.

560 Consequently, it could significantly enhance long-term aqueous membrane stability
561 (i.e., anti-swelling ability) via robustly forming stable nano-channels with
562 space-confined sub-nanometer dimension after stronger covalent cross-linking with
563 TU and MPD molecules.

564 The covalently cross-linked nano-channels presented an enhanced sieving ability
565 for inorganic salts and organic micro-pollutants. Due to significantly suppressed
566 nano-channel dimension with excellent anti-swelling ability, enhanced size sieving
567 played a key role for efficiently sieving different-sized salts/micro-pollutants while
568 electrostatic interaction was additionally responsible for similar-sized
569 salts/micro-pollutants (Figure 7c). After covalent cross-linking with TU and MPD
570 molecules, the GOF membranes were still negatively charged, effectively rejecting
571 more negatively charged micro-pollutants via an additional electrostatic repulsion
572 mechanism. Besides size sieving and electrostatic interactions, additional steric
573 hindrance effect of MPD molecules decorated inside the nano-channels were possibly
574 responsible for high rejection, effectively sieving small-sized species (especially salts)
575 which could not transport across larger MPD-GOF nano-channels. Besides size
576 sieving, steric hindrance and electrostatic interaction, Donnan exclusion or partial
577 dehydration effect also played an important role in salt sieving process (Figure 7c).
578 For TU cross-linking, significant enhancements in rejection were achieved for salt and
579 micro-pollutants while their water permeability was moderately sacrificed due to
580 significantly decreased nano-channel size. However, for cross-linking using
581 larger-sized MPD, the MPD-GOF membranes with moderately suppressed

582 nano-channels exhibited simultaneously enhanced rejection and permeability for both
583 salts and micro-pollutants, breaking their conventional trade-off issue between
584 selectivity and permeability. Despite the suppressed dimension (from 1.23 to 0.88 nm)
585 with enhanced robustness, the hydrophobicity of MPD-GOF nano-channels was
586 enhanced due to the partial reduction of GO nano-sheet surface with less
587 oxygen-containing groups after dehydration condensation and nucleophilic addition
588 (Figure 3 and Figure 7a) and rich hydrophobic benzene rings of cross-linked MPD
589 molecules. Such a hydrophobicity enhancement inside MPD-GOF nano-channels was
590 expected to reduce their water adsorption capacity and thus dwell time[44], facilitating
591 fast water molecule transport across the space-confined nano-channels. Therefore, an
592 extraordinary enhancement in water permeability can be ascribed to such rapid
593 low-friction transport of more water molecules inside more hydrophobic
594 space-confined nano-channels (less than 1 nm) after cross-linking reaction.[64-66]
595 Similar hydrophobically enhanced space-confined transport phenomena were also
596 well confirmed via molecular dynamics simulations during water transport through
597 GO membranes,[67] carbon nanotubes[68, 69] and 2D conjugated aromatic polymer
598 membranes[70].

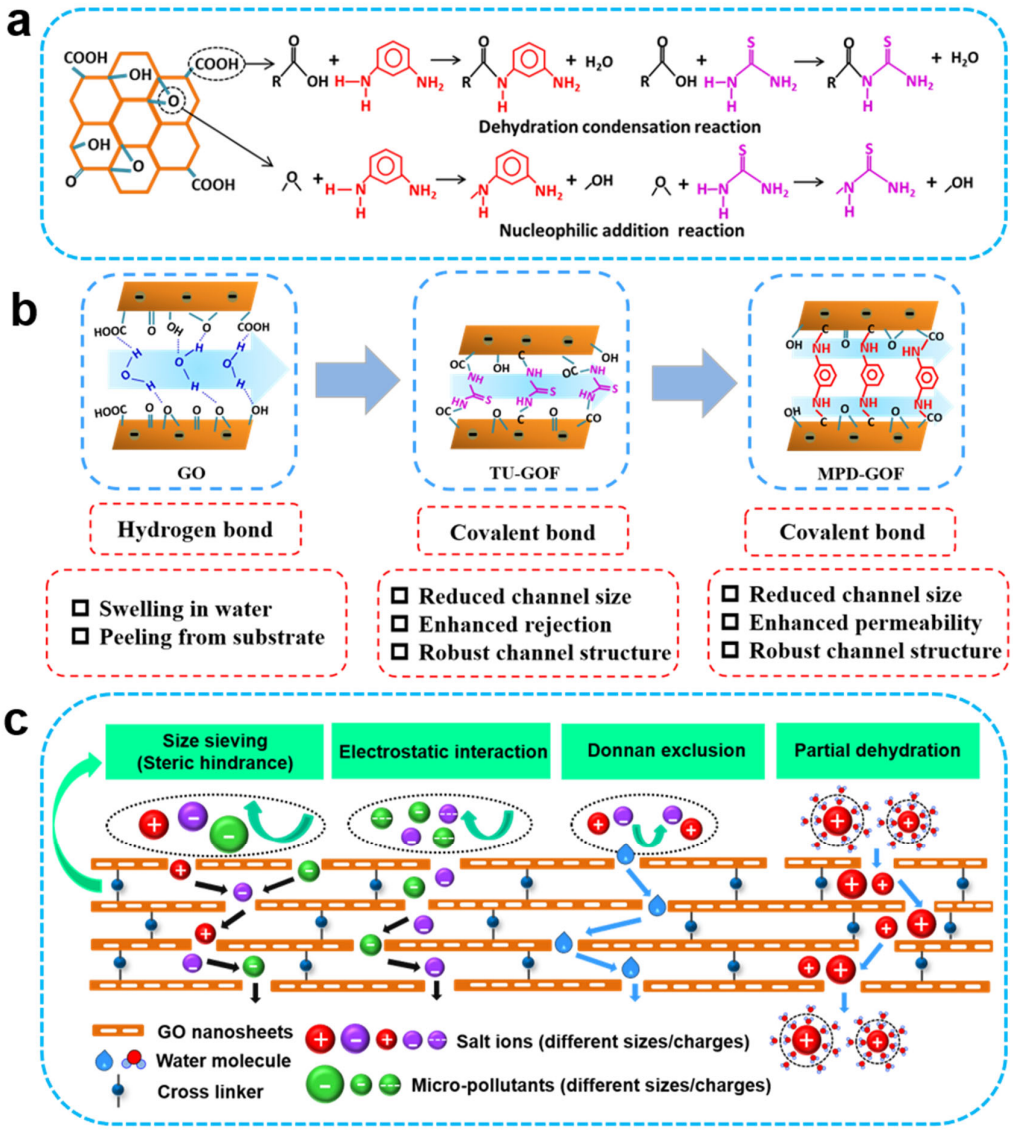

Figure 7. Schematic diagram of (a) cross-linking reactions between GO nano-sheets and TU and MPD molecules, (b) GOF membrane structures rationally designed via a molecular covalent cross-linking strategy and (c) separation mechanisms across cross-linked GO-based membranes with enhanced sieving of micro-pollutants and salts.

IMPLICATIONS

In this study, via two molecular cross-linkers, a molecule-level rational structure design strategy was proposed to fabricate ceramic-based GOF membranes, featuring enhanced selectivity or permeability with excellent long-term aqueous stability for highly efficient sieving removal of high-concentration salts and micro-pollutants. Robust nano-channels for molecule/ion sieving could be precisely designed with tailorable size and surface chemistries. Through consuming oxygenated groups on GO nano-sheet surface, such a cross-linking involved dehydration condensation between TU/MPD amine groups and GO carboxyl groups, and nucleophilic addition reaction between TU/MPD amine and GO epoxy groups. In aqueous state, incorporation of TU and MPD molecules decreased the interlayer spacing (i.e., nano-channel size) via forming more robust nano-channels which were tightly cross-linked by stronger covalent bonds in a confined dimension less than 1 nm. For TU cross-linking, due to significantly decreased nano-channel size, significant enhancements in rejection were achieved for salt (for example, 95.6% for NaCl) and micro-pollutants while their water permeability was moderately sacrificed. In contrast, for cross-linking using larger-sized MPD, the MPD-GOF membranes with moderately suppressed nano-channels showed simultaneously enhanced rejection and permeability, breaking their conventional trade-off issue between selectivity and permeability. Despite the suppressed nano-channel dimension, an extraordinary enhancement in water permeability can be ascribed to rapid low-friction transport of more water molecules inside more hydrophobic space-confined nano-channels (less than 1 nm) after

cross-linking reaction. Moreover, we demonstrated that electrostatic interaction played an important role in sieving performance especially for similar-size salts/micro-pollutants and that Donnan exclusion and partial dehydration effects were also specially present for salt sieving. This work may provide a new strategy for rational design of water-stable functional GOF membranes with alterable nano-channel size and surface chemistry for enhanced sieving performance. Considering real applications, separation of salt/micro-pollutant mixtures is very important and will be performed in our following studies. Since ceramic membranes are known to have better mechanical strength and chemical stability, future studies are needed to explore the use of ceramic-based GOF membranes for more harsh separation applications such as organic solvent and acidic or alkaline water filtrations under long-term operation.

ASSOCIATED CONTENT

Supporting Information

S1 Introduction of materials, chemicals and instruments (Tables S1-S2); S2 Characterization of raw powder (Figure S1); S3 Fabrication of α-Al_2O_3 hollow fiber ceramic substrate (Figure S2 and Table S3); S4 Optimization of α-Al_2O_3 substrate structure (Figures S3-S8); S5 Preparation of GO-based suspensions (Figures S9-S10); S6 Preparation of GO-based membranes (Figures S11-S12); S7 Chemical structure characterization of GO-based membranes (Tables S4-S6 and Figures S13-S16); S8 Stability of GO-based membranes (Figures S17-S19 and Table S7); S9 NF performance of GO-based membranes (Figures S20-S22); S10 Comparison of NF

performance (Table S8).

AUTHOR INFORMATION

Corresponding authors:

Chuyang Y. Tang (tangc@hku.hk)

Yingchao Dong (ycdong@dlut.edu.cn)

ORCID

1, Chuyang Y. Tang: 0000-0002-7932-6462

2, Yingchao Dong: 0000-0003-1409-0994

Notes

The authors declare no competing financial interest.

ACKNOWLEDGEMENTS

This work was financially supported by the National Natural Science Foundation of China (No. 21876020, No. 52070033), Youth Top-Notch Talent Program of Talent Project of Revitalizing Liaoning (No. XLYC1807250), National Key Research and Development Project (No. 2019YFA0705803), the 111 Program of Introducing Talents of Discipline to Universities (No. B13012), the Haitian Scholar Program from Dalian University of Technology, the project of Changzhou Science and Technology Bureau (No. CJ20190013) and the Key Laboratory of Industrial Ecology and Environmental Engineering (MOE) at Dalian University of Technology.

References

1. Vorosmarty, C. J.; McIntyre, P. B.; Gessner, M. O.; Dudgeon, D.; Prusevich, A.; Green, P.; Glidden, S.; Bunn, S. E.; Sullivan, C. A.; Liermann, C. R.; Davies, P. M., Global threats to human water security and river biodiversity. *Nature* **2010,** *467*, (7315), 555-561.
2. Meyer, M. F.; Powers, S. M.; Hampton, S. E., An Evidence Synthesis of Pharmaceuticals and Personal Care Products (PPCPs) in the Environment: Imbalances among Compounds, Sewage Treatment Techniques, and Ecosystem Types. *Environ. Sci. Technol.* **2019,** *53*, (22), 12961-12973.
3. Ying, G. G.; Kookana, R. S., Degradation of five selected endocrine-disrupting chemicals in seawater and marine sediment. *Environ. Sci. Technol.* **2003,** *37*, (7), 1256-1260.
4. Fu, Q. G.; Malchi, T.; Carter, L. J.; Li, H.; Gan, J.; Chefetz, B., Pharmaceutical and Personal Care Products: From Wastewater Treatment into Agro-Food Systems. *Environ. Sci. Technol.* **2019,** *53*, (24), 14083-14090.
5. Guo, J. X.; Farid, M. U.; Lee, E. J.; Yan, D. Y. S.; Jeong, S.; An, A. K., Fouling behavior of negatively charged PVDF membrane in membrane distillation for removal of antibiotics from wastewater. *J. Membr. Sci.* **2018,** *551*, 12-19.
6. Liu, S.; Tong, X.; Huang, L.; Hao, R.; Gao, H.; Chen, Y.; Crittenden, J., Study on the Transport Mechanism of a Freestanding Graphene Oxide Membrane for Forward Osmosis. *Environ. Sci. Technol.* **2020,** *54*, (9), 5802-5812.
7. Gao, J.; Sun, S. P.; Zhu, W. P.; Chung, T. S., Chelating polymer modified P84 nanofiltration (NF) hollow fiber membranes for high efficient heavy metal removal. *Water Res.* **2014,** *63*, 252-261.
8. Sun, S. P.; Hatton, T. A.; Chan, S. Y.; Chung, T. S., Novel thin-film composite nanofiltration hollow fiber membranes with double repulsion for effective removal of emerging organic matters from water. *J. Membr. Sci.* **2012,** *401*, 152-162.
9. Han, Y.; Xu, Z.; Gao, C., Ultrathin Graphene Nanofiltration Membrane for Water Purification. *Adv. Funct. Mater.* **2013,** *23*, (29), 3693-3700.
10. Werber, J. R.; Deshmukh, A.; Elimelech, M., The Critical Need for Increased Selectivity, Not Increased Water Permeability, for Desalination Membranes. *Environ. Sci. Technol. Lett.* **2016,** *3*, 112-120.
11. Lu, X. L.; Gabinet, U. R.; Ritt, C. L.; Feng, X. D.; Deshmukh, A.; Kawabata, K.; Kaneda, M.; Hashmi, S. M.; Osuji, C. O.; Elimelech, M., Relating Selectivity and Separation Performance of Lamellar Two-Dimensional Molybdenum Disulfide (MoS2) Membranes to Nanosheet Stacking Behavior. *Environ. Sci. Technol.* **2020,** *54*, (15), 9640-9651.
12. Zhang, D.; Chen, L. M.; Yao, Y. C.; Liang, F.; Qu, T.; Ma, W. H.; Yang, B.; Dai, Y. N.; Lei, Y., A novel approach to synthesize porous graphene by the transformation and deoxidation of oxygen-containing functional groups. *Chin. Chem. Lett.* **2019,** *30*, (12), 2313-2317.
13. Zhang, D.; Ye, K.; Yao, Y. C.; Liang, F.; Qu, T.; Ma, W. H.; Yang, B.; Dai, Y. N.; Watanabe, T., Controllable synthesis of carbon nanomaterials by direct current arc

discharge from the inner wall of the chamber. *Carbon* **2019,** *142*, 278-284.
14. Suk, J. W.; Piner, R. D.; An, J. H.; Ruoff, R. S., Mechanical Properties of Mono layer Graphene Oxide. *ACS Nano* **2010,** *4*, (11), 6557-6564.
15. Dikin, D. A.; Stankovich, S.; Zimney, E. J.; Piner, R. D.; Dommett, G. H. B.; Evmenenko, G.; Nguyen, S. T.; Ruoff, R. S., Preparation and characterization of graphene oxide paper. *Nature* **2007,** *448*, (7152), 457-460.
16. Nair, R. R.; Wu, H. A.; Jayaram, P. N.; Grigorieva, I. V.; Geim, A. K., Unimpeded Permeation of Water Through Helium-Leak-Tight Graphene-Based Membranes. *Science* **2012,** *335*, (6067), 442-444.
17. Mi, B. X., Graphene Oxide Membranes for Ionic and Molecular Sieving. *Science* **2014,** *343*, (6172), 740-742.
18. Joshi, R. K.; Carbone, P.; Wang, F. C.; Kravets, V. G.; Su, Y.; Grigorieva, I. V.; Wu, H. A.; Geim, A. K.; Nair, R. R., Precise and Ultrafast Molecular Sieving Through Graphene Oxide Membranes. *Science* **2014,** *343*, (6172), 752-754.
19. Li, Y.; Zhao, W.; Weyland, M.; Yuan, S.; Xia, Y.; Liu, H. Y.; Jian, M. P.; Yang, J. D.; Easton, C. D.; Selomulya, C.; Zhang, X. W., Thermally Reduced Nanoporous Graphene Oxide Membrane for Desalination. *Environ. Sci. Technol.* **2019,** *53*, (14), 8314-8323.
20. Yang, J. J.; Gong, D. A.; Li, G. H.; Zeng, G. F.; Wang, Q. Y.; Zhang, Y. L.; Liu, G. J.; Wu, P.; Vovk, E.; Peng, Z.; Zhou, X. H.; Yang, Y.; Liu, Z.; Sun, Y. H., Self-Assembly of Thiourea-Crosslinked Graphene Oxide Framework Membranes toward Separation of Small Molecules. *Adv. Mater.* **2018,** *30*, (16), 1705775.
21. Li, G. H.; Shi, L.; Zeng, G. F.; Zhang, Y. F.; Sun, Y. H., Efficient dehydration of the organic solvents through graphene oxide (GO)/ceramic composite membranes. *RSC Adv.* **2014,** *4*, (94), 52012-52015.
22. Li, G. H.; Shi, L.; Zeng, G. F.; Li, M.; Zhang, Y. F.; Sun, Y. H., Sharp molecular-sieving of alcohol-water mixtures over phenyldiboronic acid pillared graphene oxide framework (GOF) hybrid membrane. *Chem. Commun.* **2015,** *51*, (34), 7345-7348.
23. Thebo, K. H.; Qian, X. T.; Zhang, Q.; Chen, L.; Cheng, H. M.; Ren, W. C., Highly stable graphene-oxide-based membranes with superior permeability. *Nat. Commun.* **2018,** *9*, 1486.
24. Huang, H. B.; Song, Z. G.; Wei, N.; Shi, L.; Mao, Y. Y.; Ying, Y. L.; Sun, L. W.; Xu, Z. P.; Peng, X. S., Ultrafast viscous water flow through nanostrand-channelled graphene oxide membranes. *Nat. Commun.* **2013,** *4*, 2749.
25. Liu, H. Y.; Wang, H. T.; Zhang, X. W., Facile Fabrication of Freestanding Ultrathin Reduced Graphene Oxide Membranes for Water Purification. *Adv. Mater.* **2015,** *27*, (2), 249-254.
26. Sun, P. Z.; Zheng, F.; Zhu, M.; Song, Z. G.; Wang, K. L.; Zhong, M. L.; Wu, D. H.; Little, R. B.; Xu, Z. P.; Zhu, H. W., Selective Trans-Membrane Transport of Alkali and Alkaline Earth Cations through Graphene Oxide Membranes Based on Cation-pi Interactions. *ACS Nano* **2014,** *8*, (1), 850-859.
27. Yeh, C. N.; Raidongia, K.; Shao, J. J.; Yang, Q. H.; Huang, J. X., On the origin of the stability of graphene oxide membranes in water. *Nat. Chem.* **2015,** *7*, (2), 166-170.

28. Liu, G. P.; Jin, W. Q.; Xu, N. P., Graphene-based membranes. *Chem. Soc. Rev.* **2015,** *44*, (15), 5016-5030.
29. Chen, L.; Li, Y. H.; Chen, L. N.; Li, N.; Dong, C. L.; Chen, Q.; Liu, B. B.; Ai, Q.; Si, P. C.; Feng, J. K.; Zhang, L.; Suhr, J.; Lou, J.; Ci, L. J., A large-area free-standing graphene oxide multilayer membrane with high stability for nanofiltration applications. *Chem. Eng. J.* **2018,** *345*, 536-544.
30. Zhang, Y.; Zhang, S.; Chung, T. S., Nanometric Graphene Oxide Framework Membranes with Enhanced Heavy Metal Removal via Nanofiltration. *Environ. Sci. Technol.* **2015,** *49*, (16), 10235-10242.
31. Hung, W. S.; Chiao, Y. H.; Sengupta, A.; Lin, Y. W.; Wickramasinghe, S. R.; Hu, C. C.; Tsai, H. A.; Lee, K. R.; Lai, J. Y., Tuning the interlayer spacing of forward osmosis membranes based on ultrathin graphene oxide to achieve desired performance. *Carbon* **2019,** *142*, 337-345.
32. Jin, L. M.; Wang, Z. Y.; Zheng, S. X.; Mi, B. X., Polyamide-crosslinked graphene oxide membrane for forward osmosis. *J. Membr. Sci.* **2018,** *545*, 11-18.
33. Zhang, M. C.; Mao, Y. Y.; Liu, G. Z.; Liu, G. P.; Fan, Y. Q.; Jin, W. Q., Molecular Bridges Stabilize Graphene Oxide Membranes in Water. *Angew. Chem.-Int. Edit.* **2020,** *59*, (4), 1689-1695.
34. Jia, Z. Q.; Wang, Y., Covalently crosslinked graphene oxide membranes by esterification reactions for ions separation. *J. Mater. Chem. A* **2015,** *3*, (8), 4405-4412.
35. Zhang, P.; Gong, J. L.; Zeng, G. M.; Deng, C. H.; Yang, H. C.; Liu, H. Y.; Huan, S. Y., Cross-linking to prepare composite graphene oxide-framework membranes with high-flux for dyes and heavy metal ions removal. *Chem. Eng. J.* **2017,** *322*, 657-666.
36. Li, J.; Hu, M. Y.; Pei, H. C.; Ma, X. H.; Yan, F.; Dlamini, D. S.; Cui, Z. Y.; He, B. Q.; Li, J. X.; Matsuyama, H., Improved water permeability and structural stability in a polysulfone-grafted graphene oxide composite membrane used for dye separation. *J. Membr. Sci.* **2020,** *595*, 117547.
37. Dong, Y. C.; Ma, L. N.; Tang, C. Y. Y.; Yang, F. L.; Quan, X.; Jassby, D.; Zaworotko, M. J.; Guiver, M. D., Stable Superhydrophobic Ceramic-Based Carbon Nanotube Composite Desalination Membranes. *Nano Lett.* **2018,** *18*, (9), 5514-5521.
38. Chen, M. L.; Zhu, L.; Chen, J. W.; Yang, F. L.; Tang, C. Y. Y.; Guiver, M. D.; Dong, Y. C., Spinel-based ceramic membranes coupling solid sludge recycling with oily wastewater treatment. *Water Res.* **2020,** *169*, 115180.
39. Zhu, L.; Chen, M. L.; Dong, Y. C.; Tang, C. Y. Y.; Huang, A. S.; Li, L. L., A low-cost mullite-titania composite ceramic hollow fiber microfiltration membrane for highly efficient separation of oil-in-water emulsion. *Water Res.* **2016,** *90*, 277-285.
40. Xu, D. L.; Liang, H.; Zhu, X. W.; Yang, L.; Luo, X. S.; Guo, Y. Q.; Liu, Y. T.; Bai, L. M.; Li, G. B.; Tang, X. B., Metal-polyphenol dual crosslinked graphene oxide membrane for desalination of textile wastewater. *Desalination* **2020,** *487*, 114503.
41. Huang, A. S.; Feng, B., Synthesis of novel graphene oxide-polyimide hollow fiber membranes for seawater desalination. *J. Membr. Sci.* **2018,** *548*, 59-65.
42. Li, D.; Muller, M. B.; Gilje, S.; Kaner, R. B.; Wallace, G. G., Processable aqueous dispersions of graphene nanosheets. *Nat. Nanotechnol.* **2008,** *3*, (2), 101-105.
43. Cote, L. J.; Kim, J.; Zhang, Z.; Sun, C.; Huang, J. X., Tunable assembly of

graphene oxide surfactant sheets: wrinkles, overlaps and impacts on thin film properties. *Soft Matter* **2010,** *6*, (24), 6096-6101.
44. Hung, W. S.; Tsou, C. H.; De Guzman, M.; An, Q. F.; Liu, Y. L.; Zhang, Y. M.; Hu, C. C.; Lee, K. R.; Lai, J. Y., Cross-Linking with Diamine Monomers To Prepare Composite Graphene Oxide-Framework Membranes with Varying d-Spacing. *Chem. Mat.* **2014,** *26*, (9), 2983-2990.
45. Qi, B. Y.; He, X. F.; Zeng, G. F.; Pan, Y. C.; Li, G. H.; Liu, G. J.; Zhang, Y. F.; Chen, W.; Sun, Y. H., Strict molecular sieving over electrodeposited 2D-interspacing-narrowed graphene oxide membranes. *Nat. Commun.* **2017,** *8*, 825.
46. Qian, Y. L.; Zhou, C.; Huang, A. S., Cross-linking modification with diamine monomers to enhance desalination performance of graphene oxide membranes. *Carbon* **2018,** *136*, 28-37.
47. Cong, H. P.; Wang, P.; Yu, S. H., Highly Elastic and Superstretchable Graphene Oxide/Polyacrylamide Hydrogels. *Small* **2014,** *10*, (3), 448-453.
48. Cong, H. P.; Wang, P.; Yu, S. H., Stretchable and Self-Healing Graphene Oxide-Polymer Composite Hydrogels: A Dual-Network Design. *Chem. Mat.* **2013,** *25*, (16), 3357-3362.
49. Wang, Z. Y.; Dong, Y. F.; Li, H. J.; Zhao, Z. B.; Wu, H. B.; Hao, C.; Liu, S. H.; Qiu, J. S.; Lou, X. W., Enhancing lithium-sulphur battery performance by strongly binding the discharge products on amino-functionalized reduced graphene oxide. *Nat. Commun.* **2014,** *5*, 5002.
50. Kovtyukhova, N. I.; Ollivier, P. J.; Martin, B. R.; Mallouk, T. E.; Chizhik, S. A.; Buzaneva, E. V.; Gorchinskiy, A. D., Layer-by-layer assembly of ultrathin composite films from micron-sized graphite oxide sheets and polycations. *Chem. Mat.* **1999,** *11*, (3), 771-778.
51. Si, Y. R.; Sun, C. Y.; Li, D. F.; Yang, F. L.; Tang, C. Y. Y.; Quan, X.; Dong, Y. C.; Guiver, M. D., Flexible Superhydrophobic Metal-Based Carbon Nanotube Membrane for Electrochemically Enhanced Water Treatment. *Environ. Sci. Technol.* **2020,** *54*, (14), 9074-9082.
52. Chen, L.; Moon, J. H.; Ma, X. X.; Zhang, L.; Chen, Q.; Chen, L. N.; Peng, R. Q.; Si, P. C.; Feng, J. K.; Li, Y. H.; Lou, J.; Ci, L. J., High performance graphene oxide nanofiltration membrane prepared by electrospraying for wastewater purification. *Carbon* **2018,** *130*, 487-494.
53. Volkov, A. G.; Paula, S.; Deamer, D. W., Two mechanisms of permeation of small neutral molecules and hydrated ions across phospholipid bilayers. *Bioelectrochem. Bioenerg.* **1997,** *42*, (2), 153-160.
54. Chen, L.; Shi, G. S.; Shen, J.; Peng, B. Q.; Zhang, B. W.; Wang, Y. Z.; Bian, F. G.; Wang, J. J.; Li, D. Y.; Qian, Z.; Xu, G.; Liu, G. P.; Zeng, J. R.; Zhang, L. J.; Yang, Y. Z.; Zhou, G. Q.; Wu, M. H.; Jin, W. Q.; Li, J. Y.; Fang, H. P., Ion sieving in graphene oxide membranes via cationic control of interlayer spacing. *Nature* **2017,** *550*, (7676), 415-418.
55. Lind, M. L.; Suk, D. E.; Nguyen, T. V.; Hoek, E. M. V., Tailoring the Structure of Thin Film Nanocomposite Membranes to Achieve Seawater RD Membrane Performance. *Environ. Sci. Technol.* **2010,** *44*, (21), 8230-8235.

56. Zhang, M. M.; Jin, W. B.; Yang, F. L.; Duke, M.; Dong, Y. C.; Tang, C. Y. Y., Engineering a Nanocomposite Interlayer for a Novel Ceramic-Based Forward Osmosis Membrane with Enhanced Performance. *Environ. Sci. Technol.* **2020,** *54*, (12), 7715-7724.
57. Zhang, H. C.; Hou, J.; Hu, Y. X.; Wang, P. Y.; Ou, R. W.; Jiang, L.; Liu, J. Z.; Freeman, B. D.; Hill, A. J.; Wang, H. T., Ultrafast selective transport of alkali metal ions in metal organic frameworks with subnanometer pores. *Sci. Adv.* **2018,** *4*, (2), eaaq0066.
58. Razmjou, A.; Asadnia, M.; Hosseini, E.; Korayem, A. H.; Chen, V., Design principles of ion selective nanostructured membranes for the extraction of lithium ions. *Nat. Commun.* **2019,** *10*, (1), 5793.
59. Abraham, J.; Vasu, K. S.; Williams, C. D.; Gopinadhan, K.; Su, Y.; Cherian, C. T.; Dix, J.; Prestat, E.; Haigh, S. J.; Grigorieva, I. V.; Carbone, P.; Geim, A. K.; Nair, R. R., Tunable sieving of ions using graphene oxide membranes. *Nat. Nanotechnol.* **2017,** *12*, (6), 546-550.
60. Fang, S. Y.; Zhang, P.; Gong, J. L.; Tang, L.; Zeng, G. M.; Song, B.; Cao, W. C.; Li, J.; Ye, J., Construction of highly water-stable metal-organic framework UiO-66 thin-film composite membrane for dyes and antibiotics separation. *Chem. Eng. J.* **2020,** *385*, 123400.
61. Huang, H. B.; Mao, Y. Y.; Ying, Y. L.; Liu, Y.; Sun, L. W.; Peng, X. S., Salt concentration, pH and pressure controlled separation of small molecules through lamellar graphene oxide membranes. *Chem. Commun.* **2013,** *49*, (53), 5963-5965.
62. Lerf, A.; He, H. Y.; Forster, M.; Klinowski, J., Structure of graphite oxide revisited. *J. Phys. Chem. B* **1998,** *102*, (23), 4477-4482.
63. Dreyer, D. R.; Park, S.; Bielawski, C. W.; Ruoff, R. S., The chemistry of graphene oxide. *Chem. Soc. Rev.* **2010,** *39*, (1), 228-240.
64. Zhang, W.; Shi, M.; Heng, Z.; Zhang, W.; Pan, B., Soft Particles Enable Fast and Selective Water Transport through Graphene Oxide Membranes. *Nano Lett.* **2020**. DOI: 10.1021/acs.nanolett.0c02724.
65. Patel, S. K.; Ritt, C. L.; Deshmukh, A.; Wang, Z. X.; Qin, M. H.; Epsztein, R.; Elimelech, M., The relative insignificance of advanced materials in enhancing the energy efficiency of desalination technologies. *Energy Environ. Sci.* **2020,** *13*, (6), 1694-1710.
66. Kang, Y.; Xia, Y.; Wang, H. T.; Zhang, X. W., 2D Laminar Membranes for Selective Water and Ion Transport. *Adv. Funct. Mater.* **2019,** *29*, (29), 1902014.
67. Sui, X.; Ding, H. R.; Yuan, Z. W.; Leong, C. F.; Goh, K. L.; Li, W.; Yang, N.; D'Alessandro, D. M.; Chen, Y., The roles of metal-organic frameworks in modulating water permeability of graphene oxide-based carbon membranes. *Carbon* **2019,** *148*, 277-289.
68. Joseph, S.; Aluru, N. R., Why are carbon nanotubes fast transporters of water? *Nano Lett.* **2008,** *8*, (2), 452-458.
69. Hummer, G.; Rasaiah, J. C.; Noworyta, J. P., Water conduction through the hydrophobic channel of a carbon nanotube. *Nature* **2001,** *414*, (6860), 188-190.
70. Yan, Y. G.; Wang, W. S.; Li, W.; Loh, K. P.; Zhang, J., A graphene-like membrane

894 with an ultrahigh water flux for desalination. *Nanoscale* **2017,** *9*, (47), 18951-18958.
895